Journal of Mines, Metals and Fuels, *71(12C): 16-26; 2023. DOI: 10.18311/jmmf/2023/47274*

Print ISSN : 0022-2755

Journal of Mines, Metals and Fuels

Contents available at: *www.informaticsjournals.com/index.php/jmmf*

Metal Ion Sensing by Computational Characterisation of 1H-Benzo[d] Imidazole - Substituted Coumarin Derivatives

R. Shwetha[1], D. Roopa[2], Lohit Naik[3], Yin Yao[4], Yury Kapelyushin[5], Charles Mbohwa[6] and U. Mahaboob Pasha[6,7]*

[1]*Department of Physics, MES College of Science, Commerce and Arts, Bangalore - 560003, Karnataka, India*
[2]*Government First Grade College, Bannur, Mysore - 571101, Karnataka, India*
[3]*Christ University, Bangalore - 560026, Karnataka, India*
[4]*Electron Microscope Unit, Mark Wainwright Analytical Centre, UNSW Sydney, Sydney, New South Wales - 2052, Australia*
[5]*Faculty of Materials Science and Metallurgy Engineering, South Ural State University (National Research University), Prospekt Lenina, 76, Chelyabinsk, Chelyabinsk Oblast - 454080, Russia*
[6]*College of Science Engineering and Technology, University of South Africa, Pretoria, South Africa*
[7]*Presidency University, Bangalore – 560064, Karnataka, India; mahaboobpasha@presidencyuniversity.in*

Abstract

The present work presents a computational investigations on a 3-(2-(1H-benzo[d]imidazol-1-yl)-1-((6-chloro-2-oxo-2H-chromen-4-yl)methoxy)ethyl)-6-chloro-2H-chromen-2-one (3ClOX) using Density Functional Theory (DFT) with the B3LYP functional and 6-311G basis set. The optimised geometry reveals key structural characteristics, such as bond lengths, bond angles and dihedral angles, which provide insights into the molecule's aromatic and planar regions. Mulliken charge distribution analysis in a vacuum, hexene and Dimethyl Sulfoxide (DMSO) solvents highlights the solvent influence on electron density, with polar solvents showing enhanced charge separation. Frontier Molecular Orbital (FMO) analysis indicates an energy gap (ΔE) of 3.239 eV between the Highest Occupied Molecular Orbital (HOMO) and Lowest Unoccupied Molecular Orbital (LUMO), suggesting moderate molecular stability and reactivity. The molecule's global reactivity descriptors, including ionisation potential, electron affinity, chemical hardness and electrophilicity, reveal its potential for charge transfer processes and interactions in chemical and electrochemical systems. The Electrostatic Potential (ESP) and Molecular Electrostatic Potential (MESP) mappings further demonstrate electron density concentration and depletion regions, essential for understanding the molecule's reactivity. The findings suggest that 3ClOX could be a promising candidate for applications in photonics, charge-transfer systems and electrochemical sensors, owing to its balanced stability, moderate reactivity and strong electrophilic nature. Overall, the results suggest that the 3ClOX molecule could serve as a sensor for detecting metal ions.

Keywords: *Coumarin Derivative, FMO, MESP, Mulliken, UV-Vis*

**Author for correspondence*

1.0 Introduction

Coumarins are benzopyran-1-one compounds characterized by a fused pyrone and benzene ring, with the pyrone's carbonyl group positioned at the second carbon[1-3]. According to the latest International Union of Pure and Applied Chemistry (IUPAC) nomenclature, this structure is also referred to as 2H-chromen-2-one. The coumarin framework consists of six peripheral C–H bonds, a C=O group and a rigid C=C bond that remains in the cis-conformation, which prevents the typical trans–cis isomerisation seen in vinylic compounds. This rigidity allows for targeted post-functionalization at the 6 or 7 positions on the phenyl ring, or the 3 or 4 positions on the vinyl group, making such modifications both chemically feasible and appealin[4-6].

In recent years, colourimetric and fluorescence techniques have gained prominence in clinical diagnostics, environmental monitoring and biological studies, thanks to their high sensitivity, selectivity, simplicity, non-destructive nature and ability to provide rapid and direct optical feedback[7]. The intrinsic optical and photochemical properties of many coumarin derivatives make them ideal candidates for use as signalling molecules in sensors and sophisticated photophysical systems. The lactone group in coumarins locks the C=C bond in a cis-conformation, thereby enhancing their fluorescence, quantum yield and photostability under UV light. While the parent coumarin compound itself shows weak or negligible fluorescence, appropriate substitutions often result in strong fluorescence within the visible light spectrum[8-11].

Coumarins exhibit a range of desirable optical characteristics, such as high fluorescence quantum yield, strong light absorption and large stokes shifts, which have attracted significant attention for photonic applications[12]. Their use as fluorescent probes and optical brighteners stems directly from these valuable properties. Various research efforts have demonstrated the effectiveness of coumarin and its derivatives in a wide range of applications. In recent years, they have been extensively studied for photonic and electronic uses, including solar energy harvesting, charge-transfer agents, fluorescence probes, optical brighteners, Organic Light Emitting Diodes (OLEDs) and nonlinear optical materials[13-15]. These applications are driven by coumarins' inherent photophysical properties, broad spectral range, stability and solubility, with their performance depending heavily on the rigidity of the molecular structure and the nature and position of substituents.

2. Analysis of Density Functional Theory

The bis-chloro coumarin derivatives, namely 3-(2-(1H-benzo[d]imidazol-1-yl)-1-((6-chloro-2-oxo-2H-chromen-4-yl)methoxy)ethyl)-6-chloro-2H-chromen-2-one (3ClOX) is selected from the literature[16]. The molecular structure of the 3ClOX is given in Figure 1.

Structural and theoretical analyses of 3ClOX were carried out using the GaussView 5.0 and Gaussian 09 W software packages[17]. The geometry optimisation was performed using DFT with the B3LYP functional and the 6-311G basis set. The B3LYP/6-311G methodology was applied throughout the analysis. FMO analysis was conducted in both vacuum and liquid-phase environments, allowing for a detailed examination of 3ClOX's electronic structure, thermodynamic properties and optical behaviour. This approach provided valuable insights into the molecule's electronic transitions and oscillatory strengths under varying conditions, contributing to a deeper understanding of its potential applications.

The energy levels of the HOMO and LUMO were analysed across different media, offering insights into critical molecular properties such as ionisation

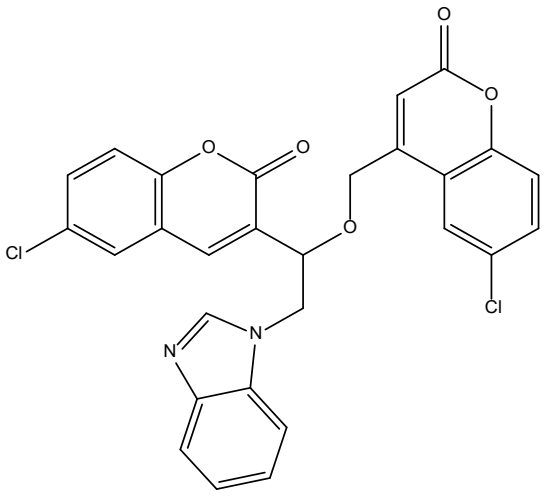


Figure 1. Molecular structure of the 3ClOX molecule.

potential, electron affinity, chemical hardness and electrophilic index. Additionally, DFT was employed to map the Total Electron Density (TED), Electrostatic Potential (ESP) and Molecular Electrostatic Potential (MEP) surfaces. Contour mapping in both vacuum and solvent conditions provided further insight into 3ClOX's molecular interactions, enhancing our understanding of its behaviour in different environments.

3.0 Results and Discussions

3.1. Structure and Geometric Properties

The structural design of 3ClOX was initially generated in GaussView-5 and subsequently optimised using Gaussian 09 software. The optimisation process, conducted with the "opt" keyword, utilised the B3LYP functional and the 6-311G basis set[18]. Starting from standard parameters, the Gaussian program iteratively minimised the geometry to identify the configuration with the lowest energy, resembling the molecular structure at its energy minimum. The resulting optimised molecular geometries of 3ClOX are depicted in Figure 2, providing a visual representation of the molecule's conformational characteristics.

The structural analysis of the molecule 3ClOX reveals detailed insights into its bond lengths, bond angles, and dihedral angles, as presented in Table 1. Key bond lengths include the C1-O12 bond at 1.227 Å, typical of a strong C=O bond, while the C1-O13 bond measures 1.427 Å, characteristic of a C-O single bond. The O13-C5 bond length is 1.384 Å, indicating partial double bond character due to resonance. Bonds between C1-C2 (1.454 Å) and C2-C3 (1.360 Å) are consistent with those in aromatic systems. The bond between C8 and Cl54 is longer, at 1.828 Å, reflecting chlorine's larger atomic radius. Other notable bond lengths include C3-C16 (1.507 Å), C16-O19 (1.460 Å), and O19-C20 (1.463 Å), which define the chromenone moiety. The bond angles reveal the molecular structure in more detail. The O12-C1-O13 angle is 117.75°, close to the ideal sp^2 hybridised angles found in carbonyl compounds, while C1-O13-C5 measures 122.30°, indicating the geometry around the ether oxygen. The O13-C1-C2 bond angle is 115.33°, consistent with resonance effects in the system. Bond angles around the C8 atom, such as C9-C8-Cl54 (118.71°) and C7-C8-Cl54 (119.06°), reflect the planar geometry expected in chloro-substituted aromatic systems. The angles C16-O19-C20 (116.64°) and O19-C20-C37 (103.15°) indicate distortions caused by larger atoms like oxygen and chlorine. Dihedral angles provide a three-dimensional perspective of the molecule. The H17-O16-O19-C20 dihedral angle is 58.80°, suggesting a non-planar arrangement around the oxygen atoms, while the H21-C20-C37-H38 angle of 166.98° indicates a nearly anti-periplanar configuration, implying that these atoms are almost aligned in a straight line. Highly planar arrangements are observed in the C3-C16-O19-C20 (179.09°) and C16-O19-C20-C37 (178.30°) angles within the chromenone system. Twists are noted around certain bonds, such as H38-C37-N53-C41 (106.38°) and O19-C20-C37-N53 (156.82°), reflecting steric influences on the molecular structure.

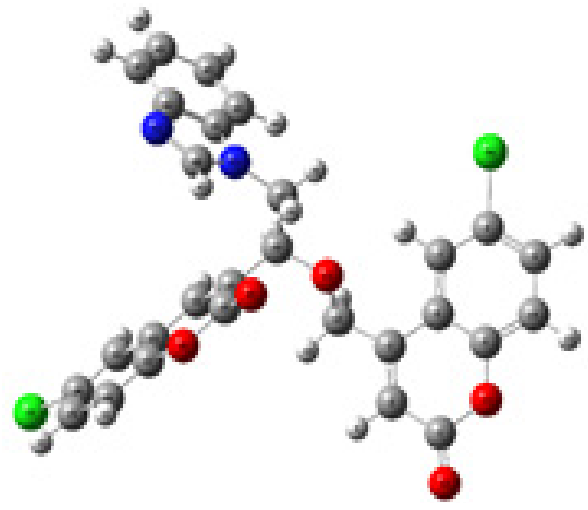


Figure 2. Optimised molecular geometry of the 3ClOX molecule.

The bond lengths and angles suggest a primarily planar geometry in the aromatic regions, with subtle twists in the overall structure due to steric hindrance. These structural details provide a comprehensive understanding of the molecule's electronic properties, chemical reactivity and its potential applications in fields such as photonics and biochemistry[19].

The Mulliken atomic charge distributions[20] of each atomic site in 3ClOX were investigated using DFT with the B3LYP/6-311G method in three different environments: vacuum, hexene and DMSO which are useful for various atomic and molecular fields. Table 2 presents the Mulliken charge distribution of each atom in 3ClOX

Table 1. Estimation of bond length (Å), bond angle (°) and dihedral angle of 3ClOX using DFT/B3LYP/6-311G.

Atoms	Bond length (Å)	Atoms	Bond Angle (°)	Atoms	Dihedral Angle (°)
C1-O12	1.227	O12-C1-O13	117.75	H17-O16-O19-C20	58.80
C1-O13	1.427	C1-O13-C5	122.30	H21-C20-C37-H38	166.98
O13-C5	1.384	O13-C1-C2	115.33	H38-C37-N53-C41	106.38
C1-C2	1.454	C2-C3-C6	119.65	C3-C16-O19-C20	179.09
C2-C3	1.360	C9-C8-Cl54	118.71	C16-O19-C20-C37	178.30
C8-Cl54	1.828	C7-C8-Cl54	119.06	O19-C20-C37-N53	156.82
C3-C6	1.456	C3-C16-O19	107.65		
C3-C16	1.507	C16-O19-C20	116.64		
C16-O19	1.460	O19-C20-C37	103.15		
O19-C20	1.463	C20-C37-N53	112.41		
C20-H21	1.100	O19-C20-C25	114.14		
O19-C20	1.439	N53-C40-N52	113.28		
C20-C37	1.543	C40-N52-C42	105.15		
C37-N53	1.458	N52-C42-C41	109.89		
N53-C40	1.392	C42-C41-N53	105.31		
C40-N52	1.323	H39-C37-H38	107.81		
N52-C42	1.407				
C42-C41	1.420				
C41-N53	1.400				
C20-C25	1.518				
C30-Cl55	1.819				
C25-C26	1.469				
C26-O35	1.222				
C26-O36	1.427				

different mediums, highlighting the solvent influences. Figures 3 and 4 graphically illustrate the variation in charge distribution across molecules. The Mulliken atomic charges of the molecule 3-(2-(1H-benzo[d] imidazol-1-yl)-1-((6-chloro-2-oxo-2H-chromen-4-yl) methoxy)ethyl)-6-chloro-2H-chromen-2-one. These were calculated in three different environments: vacuum, hexene and DMSO. These charges provide insight into

Table 2. Mulliken atomic charges by DFT/ B3LYP/6-311G in vacuum and solvent medium

Atom Label	Vacuum	Hexene	DMSO
1C	0.509	0.559	1.408
2C	-0.190	-0.140	0.709
3C	0.131	0.181	1.030
4H	0.202	0.252	1.101
5C	0.284	0.334	1.183
6C	0.087	0.137	0.986
7C	-0.157	-0.107	0.742
8C	-0.265	-0.215	0.634
9C	-0.095	-0.045	0.804
10H	0.158	0.208	1.057
11H	0.161	0.211	1.060
12O	-0.408	-0.358	0.491
13O	-0.526	-0.476	0.373
14C	-0.150	-0.100	0.749
15H	0.161	0.211	1.060
16C	-0.082	-0.032	0.817
17H	0.131	0.181	1.030
18H	0.157	0.207	1.056
19O	-0.488	-0.438	0.411
20C	0.090	0.140	0.989
21H	0.148	0.198	1.047
22C	0.285	0.335	1.184
23C	0.148	0.198	1.047
24C	-0.281	-0.231	0.618
25C	-0.013	0.037	0.886
26C	0.514	0.564	1.413
27H	0.211	0.261	1.110
28C	-0.146	-0.096	0.753
29C	-0.088	-0.038	0.811
30C	-0.264	-0.214	0.635
31C	-0.147	-0.097	0.752

32H	0.170	0.220	1.069
33H	0.170	0.220	1.069
34H	0.171	0.221	1.070
35O	-0.395	-0.345	0.504
36O	-0.517	-0.467	0.382
37C	-0.130	-0.080	0.769
38H	0.189	0.239	1.088
39H	0.179	0.229	1.078
40C	0.226	0.276	1.125
41C	0.199	0.249	1.098
42C	0.061	0.111	0.960
43H	0.193	0.243	1.092
44C	-0.083	-0.033	0.816
45C	-0.138	-0.088	0.761
46C	-0.139	-0.089	0.760
47C	-0.077	-0.027	0.822
48H	0.142	0.192	1.041
49H	0.134	0.184	1.033
50H	0.131	0.181	1.030
51H	0.150	0.200	1.049
52N	-0.406	-0.356	0.493
53N	-0.566	-0.516	0.333
54Cl	0.119	0.169	1.018
55Cl	0.137	0.187	1.036

how the distribution of electron density varies across the atoms of the molecule depending on the surrounding medium, influencing the molecule's reactivity, polarity, and intermolecular interactions. In a vacuum, the electron density is more localised, with charges typically smaller in magnitude compared to those in solvent environments. For instance, the charge on C1 in vacuum is 0.509, which increases slightly to 0.559 in hexene and significantly to 1.408 in DMSO. This trend suggests that C1 becomes more positive as the environment becomes more polar, indicating enhanced electron withdrawal in polar solvents like DMSO. Similarly, atoms like C2 and C3 show an increase in positive charge from vacuum to DMSO. C2 shifts from -0.190 in vacuum to -0.140 in hexene and further to 0.709 in DMSO, reflecting increased electron depletion in polar environments. C3 follows a similar pattern, moving from 0.131 in vacuum to 1.030 in DMSO. Hydrogen atoms (H4, H10, H11) generally exhibit small positive charges across all environments, but their charge magnitude increases in more polar solvents. For example, H4 has a charge of 0.202 in vacuum, rising to 1.101 in DMSO, indicating stronger interactions with electron-withdrawing groups in polar solvents. The oxygen atoms (O12, O13, O19)

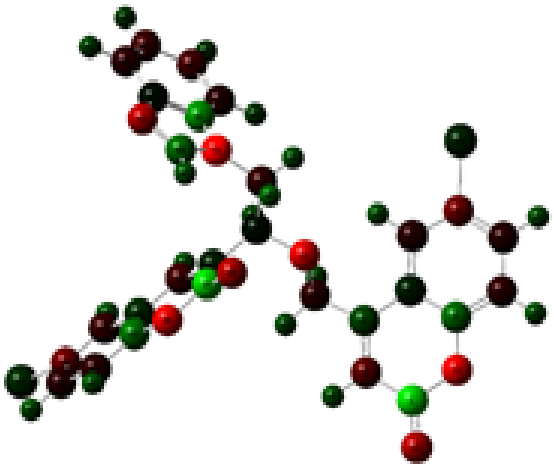


Figure 3. Mulliken charge distribution on the 3ClOX molecule.

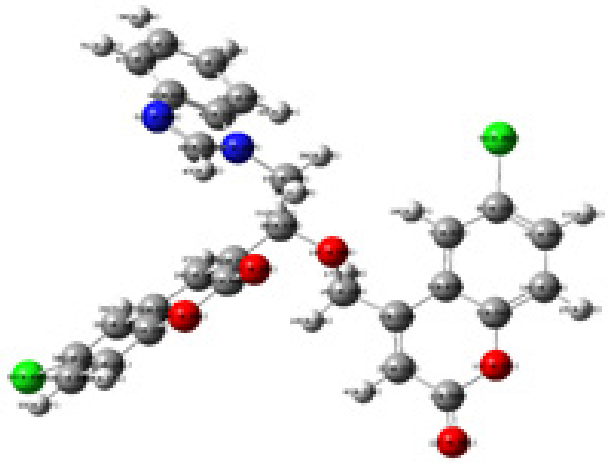


Figure 4. A statistical representation of Mulliken charge distribution on the 3ClOX molecule in the gas phase.

consistently display negative charges, as expected due to their high electronegativity. However, the magnitude of these charges also varies with the environment. O12 has a charge of -0.408 in vacuum, decreasing to -0.358 in hexene, and further to 0.491 in DMSO, reflecting changes in electron density as the solvent polarity increases. Chlorine atoms (Cl54, Cl55) show relatively small positive charges in all environments, but they also experience a notable increase in DMSO. Cl54, for instance, has a charge of 0.119 in vacuum, increasing to 0.169 in hexene and 1.018 in DMSO. This suggests that the chlorine atoms are more electron-deficient in polar solvents. The varying Mulliken charges indicate how the molecule's electronic structure adapts to different environments. In non-polar solvents like hexene, the charges are generally less extreme, suggesting that the molecule retains a more neutral distribution of electron density. In contrast, in DMSO, a highly polar solvent, many atoms become more positively or negatively charged, suggesting stronger electron withdrawal or donation. This behaviour can affect molecular interactions, such as hydrogen bonding, dipole interactions and the overall stability of the molecule in solution. The Mulliken charge analysis highlights that the molecule's electron distribution is highly sensitive to the surrounding environment, with polar solvents like DMSO significantly enhancing charge separation. This suggests that the molecule may exhibit different reactivity, solubility, and interaction patterns in different solvents, which is crucial for its potential applications in areas like catalysis, sensing or photonic materials[21].

3.2 Frontier Molecular Orbitals (FMO) and Quantum Chemical Simulation

The FMO enables recognition of the electron charge transfer between the donor and acceptor group by the π-conjugate. The HOMO (electron-donating) is directly associated with the ionisation potential, even as the LUMO (electron-accepting) is associated with the electron affinity of the compound. The plot of FMO helps us to have higher information on the nature of

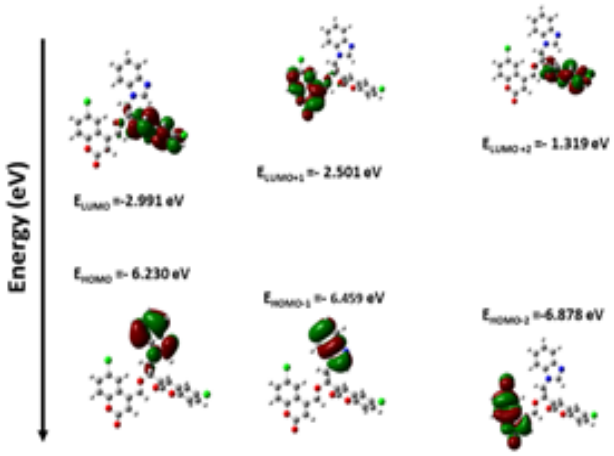


Figure 5. 3D representation of frontier molecular orbital of 3ClOX in DMSO using the DFT method.

the chemical structure and chemical reaction of the molecule[9,22] HOMO, HOMO-1, HOMO-2 are the orbitals that present π-bonding symmetry and LUMO, LUMO+1, LUMO+2 are molecular orbitals that show π* antibonding symmetry. Figure 5 indicates a 3D representation of frontier molecular orbital in different mediums using the DFT method with B3LYP functional and 6-311G basis set in which the greenish area indicates the positive region and the reddish area shows the negative region of the molecular orbital.

The energy gap (E_g) has been analysed using the equation (1) given below, which gives the energy gap (E_g) between HOMO to LUMO. The E_g in DMSO medium shows the largest energy gap of 4.205 eV, the energy gap of HOMO-1 to LUMO+1 is 6.073 eV and the E_g between HOMO+2 to LUMO-2 is 6.540 eV.

The global electrochemical reactivity descriptors[23] of the molecule 3-(2-(1H-benzo[d]imidazol-1-yl)-1-((6-chloro-2-oxo-2H-chromen-4-yl)methoxy) ethyl)-6-chloro-2H-chromen-2-one have been calculated, providing insights into its electronic and chemical behaviour and are given in Table 3. These parameters are crucial in predicting the molecule's reactivity, stability and potential interactions in various chemical and electrochemical processes. The energy of the highest occupied molecular orbital (E_{HOMO}) is -6.23 eV and the energy of the lowest unoccupied molecular orbital (E_{LUMO}) is -2.991 eV. The energy gap (ΔE) between these orbitals is 3.239 eV. This energy gap is an important indicator of the molecule's stability and reactivity, with a smaller gap suggesting higher reactivity and easier electron transfer, while a larger gap indicates a more stable molecule with lower reactivity. A gap of 3.239 eV indicates moderate stability and suggests that the molecule may participate in charge transfer processes under suitable conditions.

The Ionisation Potential (IP) of the molecule is 6.230 eV, which represents the energy required to remove an electron from the HOMO. This relatively high value suggests that the molecule is stable and resistant to losing electrons, making it less likely to undergo oxidation. The Electron Affinity (EA) is 2.991 eV, which indicates the energy released when an electron is added to the LUMO. A positive EA value suggests that the molecule is capable of accepting electrons, making it suitable for reduction processes. The chemical hardness (η) of the molecule is 1.620 eV, which quantifies the resistance of the molecule to charge transfer. A higher hardness value indicates that the molecule is less reactive, while a lower value suggests higher reactivity. The moderate hardness value of 1.620 eV suggests the molecule has a balanced reactivity profile, being neither too reactive nor too inert. Electronegativity (χ) is calculated as 4.611 eV, which is a measure of the molecule's tendency to attract electrons. A higher electronegativity value suggests a greater ability to pull electrons towards itself, implying that this molecule can act as an electron acceptor in chemical reactions. The chemical potential (μ) of the molecule is -4.611 eV, which represents the tendency of the molecule to gain or lose electrons. The negative value indicates that the molecule prefers to gain electrons, which aligns with its positive electron affinity. The softness (s) of the molecule, which is the inverse of hardness, is 0.309 eV^{-1}. A lower softness value corresponds to a harder, less reactive molecule, meaning this molecule has moderate softness and reactivity. The electrophilicity index (ω), a measure of the molecule's ability to accept electrons, is 6.563 eV. This relatively high value suggests that the molecule is a strong electrophile, meaning it has a high potential to accept electrons in reactions. The global electrochemical reactivity descriptors indicate that the molecule is moderately reactive with a balanced stability profile. It has the potential to participate in both oxidation and reduction reactions, although it is more inclined to accept electrons due to its positive electron affinity and high electrophilicity index. These properties make the molecule a suitable candidate for applications in charge-transfer systems, photonics, and

Table 3. Global electrochemical reactivity descriptor parameter of 3ClOX.

E_{HOMO} (eV)	E_{LUMO} (eV)	ΔE (eV)	IP (eV)	EA (eV)	h (eV)	c (eV)	M (eV)	s (eV^{-1})	ω (eV)
−6.230	-2.991	3.239	6.230	2.991	1.620	4.611	-4.611	0.309	6.563

electrochemical sensors. The moderate HOMO-LUMO gap, combined with its electrophilic nature, suggests that the molecule could be involved in various chemical and electrochemical processes with moderate reactivity and stability.

3.3 Electrostatic Potential (ESP), Total Electron Density (TED) and Molecular Electrostatic Potential (MESP) Studies

Three-dimensional mappings of ESP, TED and MESP were generated using DFT with the B3LYP functional and 6-311G basis set, as shown in Figures 6 to 8. These visual representations of the 3ClOX structure were analysed using surface contouring in Gaussian-09W software. The

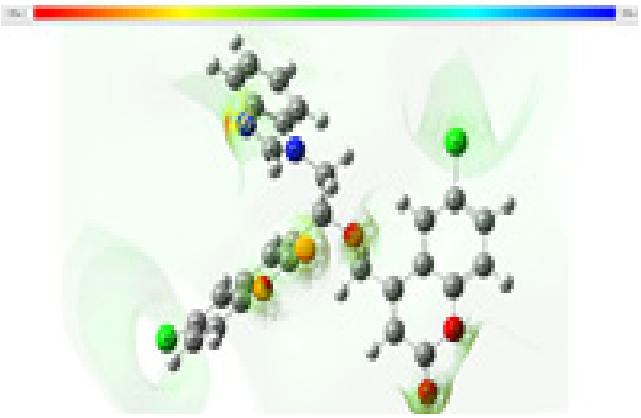


Figure 6. Electrostatic potential mapping of 3ClOX molecule in vacuum.

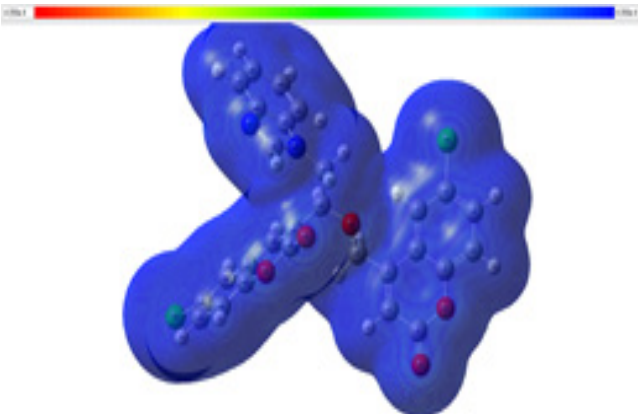


Figure 7. Total electron density mapping of 3ClOX molecule in vacuum.

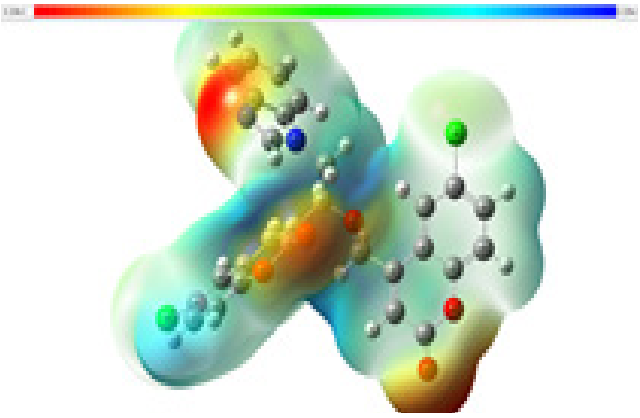


Figure 8. Molecular electrostatic potential mapping of 3ClOX molecule in vacuum.

ESP mapping illustrates the interaction energy between the molecule's electron cloud and positive point charges near the nuclei. In Figure 6, the ESP mapping of the 3ClOX molecule reveals an energy range from -1.865×10^{-2} eV to 1.865×10^{-2} eV in a vacuum. Notably, oxygen atoms O12, O13, and O19 exhibit the most negative potential values (-0.114 eV) in a vacuum, represented by red regions, highlighting their susceptibility to nucleophilic attacks. Additionally, nitrogen atoms 52N and 53N show positive potential values (0.162 eV and 0.172 eV), marked in yellow, indicating possible sites for electrophilic interactions.

The TED mapping, shown in Figure 7, provides a theoretical framework to estimate the total electron density, giving insights into the molecule's shape, charge distribution and electron delocalisation. The electron density of 3ClOX in vacuum is $\pm4.050\times10^{-4}$ Hartrees, displaying a relatively uniform distribution across the surface of the molecule. This uniformity aids in understanding various molecular properties, including chemical bonding and potential reactivity.

Figure 8 presents the MESP mapping of 3ClOX in vacuum, showing contour values ranging from -6.328×10^{-2} eV to 6.328×10^{-2} eV. The red regions around oxygen atoms O12, O13, O35, and O36 indicate areas of lower energy, making these atoms more susceptible to nucleophilic attacks. In contrast, the 1H-benzo[d] imidazole group attached to nitrogen atoms 52N and 53N displays a positive charge (blue region), making them likely sites for electrophilic attacks. The yellow areas surrounding carbon atoms represent nucleophilic

sites, while the light blue regions near hydrogen atoms signify their role as electron donors. These mappings, obtained through DFT/B3LYP/6-311G, offer detailed insights into the electronic and reactive properties of the 3ClOX molecule, highlighting potential sites for chemical interactions[24].

4.0 Conclusion

The computational analysis of the 3ClOX molecule using DFT provides valuable insights into its potential for metal ion detection. With an energy gap of 3.239 eV, the molecule exhibits moderate chemical stability, which is crucial for maintaining structural integrity during interactions with metal ions. The solvent-dependent Mulliken charge distribution highlights the importance of the surrounding environment in influencing electron density, which plays a significant role in metal ion binding. The FMO analysis and global reactivity descriptors suggest that 3ClOX has favourable charge transfer properties, making it an excellent candidate for selective metal ion detection. Electrostatic potential mappings reveal distinct electrophilic regions that are likely to interact with metal ions, providing specific sites for metal ion coordination. Overall, 3ClOX shows great promise in sensor applications, particularly in detecting metal ions in various environmental and industrial contexts due to its well-balanced stability, reactivity and specific binding characteristics.

5.0 References

1. Stefanachi A, Leonetti F, Pisani L, Catto M, Carotti A. Coumarin: A natural, privileged and versatile scaffold for bioactive compounds. Molecules. 2018; 23:250. https://doi.org/10.3390/molecules23020250
2. Zhu H, Fan J, Wang B, Peng X. Fluorescent, MRI and colorimetric chemical sensors for the first-row d-block metal ions. Chem Soc Rev. 2015; 44:4337. https://doi.org/10.1039/C4CS00285G
3. Veale EB, Gunnlaugsson T. Fluorescent sensors for ions based on organic structures. Annu Rep Prog Chem Sect B. 2010; 106:376.
4. Khan D, Shaily A. Coumarin-based fluorescent sensors. Appl Organomet Chem. 2023; 37(7). https://doi.org/10.1002/aoc.7138
5. Tasior M, Kim D, Singha S, Krzeszewski M, Ahn KH, Gryko DT. π-Expanded coumarins: Synthesis, optical properties and applications. J Mater Chem C. 2015; 3:1421. https://doi.org/10.1039/C4TC02665A
6. Cooke D, Fitzpatrick B, O'Kennedy R, McCormack T, Egan D. In: O'Kennedy R, Thornes RD, editors. Coumarins: Biology, applications and mode of action. Chichester: John Wiley & Sons. 1997; 303.
7. Sanchez-de-Armas R, Miguel MAS, Oviedo J, Sanz JF. Coumarin derivatives for dye-sensitized solar cells: A TD-DFT study. Phys Chem Phys. 2012; 14:225. https://doi.org/10.1039/C1CP22058F
8. Shaily AK, Ahmed N. Imidazo[1,2-a]pyridine-substituted coumarin as a selective ratiometric sensor for Cu^{2+} ion. Supramol Chem. 2016; 29:146. https://doi.org/10.1080/10610278.2016.1190453
9. Shiraishi T, Kagechika H, Hirano T. 6-Arylcoumarins: versatile scaffolds for fluorescent sensors. New J Chem. 2015; 39:8389. https://doi.org/10.1039/C5NJ01609F
10. Shaily AK, Ahmed N. Indirect approach for CN-Detection: Development of "naked-eye" Hg^{2+}-induced turn-off fluorescence and turn-on cyanide sensing by the Hg^{2+} displacement approach. Ind Eng Chem Res. 2017; 56:6358.
11. Jivaramonaikul W, Rashatasakhon P, Wanichwecharungruang S. UVA absorption and photostability of coumarins. Photochem Photobiol Sci. 2010; 9:1120. https://doi.org/10.1039/c0pp00057d
12. Qian R, Tong H, Huang C, Li J, Tang Y, Wang R, Lou K, Wang W. A donor-acceptor triptycene-coumarin hybrid dye featuring a charge separated excited state and AIE properties. Org Biomol Chem. 2016; 14:5007. https://doi.org/10.1039/C6OB00822D
13. Hirano T, Hiromoto K, Kagechika H. Development of a library of 6-aryl coumarins as candidate fluorescent sensors. Org Lett. 2007; 9:1315. https://doi.org/10.1021/ol070142z
14. Feuster EK, Glass TE. Detection of amines and unprotected amino acids in aqueous conditions by formation of highly fluorescent iminium ions. J Am Chem Soc. 2003; 125:16174. https://doi.org/10.1021/ja036434m
15. Saleh N, Al-Soud YA, Nau WM. Novel fluorescent pH sensor based on coumarin with piperazine and imidazole substituents. Spectrochim Acta A Mol Biomol Spectrosc. 2008; 71(3):818. https://doi.org/10.1016/j.saa.2008.02.004
16. Savanur HM, Pawashe GM, Kim KM, Kalkhambkar RG. Synthesis and molecular modelling studies of coumarin-and I-aza-coumarin-linked miconazole analogues and their antifungal activity. Chemistry Select. 2018; 3(33):9648-53. https://doi.org/10.1002/slct.201801408
17. Frisch MJ, Trucks GW, Schlegel HB, Scuseria GE, Robb MA, Cheeseman JR, *et al.* Gaussian-09, Revision B.01. Wallingford, CT: Gaussian, Inc. 2010.

18. Raghavachari K. Perspective on density functional thermochemistry. III. The role of exact exchange. J Chem Phys. 2000; 98. https://doi.org/10.1007/978-3-662-10421-7_60
19. Shirley WA, Hoffmann R, Mastryukov VS. An approach to understanding bond length/bond angle relationships. J Phys Chem. 1995; 99(12):4025-33. https://doi.org/10.1021/j100012a024
20. Tsuzuki S, Uchimaru T, Tanabe K, Yliniemela A. Comparison of atomic charge distributions obtained from different procedures: Basis set and electron correlation effects. J Mol Struct Theochem. 1996; 365(2-3):81-8. https://doi.org/10.1016/0166-1280(96)04500-9
21. Petrushenko IK. A DFT study of hydrogen absorption onto h-BN: Boron doping effects. J Nano Electron Phys. 2019; 11(2): 02024-1-02024-5. 10.21272/jnep.11(2).02024
22. Zara Z, Iqbal J, Ayub K, Irfan M, Mahmood A, Khera RA, Eliasson B. A comparative study of DFT calculated and experimental UV/Visible spectra for thirty carboline and carbazole-based compounds. J Mol Struct. 2017; 1149:282-98. https://doi.org/10.1016/j.molstruc.2017.07.093
23. Nogueira JJ, González L. Computational photophysics in the presence of an environment. Annu Rev Phys Chem. 2018; 69:473-97. https://doi.org/10.1146/annurev-physchem-050317-021013
24. Tichnell CR, Shultz DA, Popescu CV, Sokirniy I, Boyle PD. Synthesis, characterization, and photophysical studies of an iron (III) catecholate-nitronylnitroxide spin-crossover complex. Inorg Chem. 2015; 54(9):4466-74. https://doi.org/10.1021/acs.inorgchem.5b00298